# Therapeutic effects of PDGF-AB/BB against cellular senescence in human intervertebral disc

Changli Zhang[1, 2], Martha Elena Diaz-Hernandez[1, 2], Takanori Fukunaga[1, 2], Shenoy Sreekala[1,2], Sangwook Tim Yoon[3], Lisbet Haglund[4], Hicham Drissi[1, 2]

[1]Department of Orthopaedics, Emory University School of Medicine, Atlanta, GA, USA

[2]Atlanta VA Medical Center, Decatur, GA, USA

[3]Emory Orthopaedics & Spine Center, Atlanta, GA, USA

[4]Department of Surgery, McGill University, Montreal, Qc., Canada

Corresponding author:

Hicham Drissi, PhD

hicham.drissi@emory.edu

Key words: PDGF, cellular senescence, intervertebral disc degeneration, irradiation, oxidative stress, reactive oxygen species.

**Abstract**

Cellular senescence, characterized by a permanent state of cell cycle arrest and a secretory phenotype contributing to inflammation and tissue deterioration, has emerged as a target for age-related interventions. Accumulation of senescent cells is closely linked with intervertebral disc (IVD) degeneration, a prevalent age-dependent chronic disorder causing low back pain. Previous studies have highlighted that platelet-derived growth factor (PDGF) mitigated IVD degeneration through anti-apoptosis, anti-inflammation, and pro-anabolism. However, its impact on IVD cell senescence remains elusive. In this study, human NP and AF cells derived from aged, degenerated IVDs were treated with recombinant human (rh) PDGF-AB/BB for 5 days and changes of transcriptome profiling were examined through mRNA sequencing. NP and AF cells demonstrated similar but distinct responses to the treatment. However, the effects of PDGF-AB and BB on human IVD cells were comparable. Specifically, PDGF-AB/BB treatment resulted in downregulation of gene clusters related to neurogenesis and response to mechanical stimulus in AF cells while the downregulated genes in NP cells were mainly associated with metabolic pathways. In both NP and AF cells, PDGF-AB and BB treatment upregulated the expression of genes involved in cell cycle regulation, mesenchymal cell differentiation, and response to reduced oxygen levels, while downregulating the expression of genes related to senescence associated phenotype, including oxidative stress, reactive oxygen species (ROS), and mitochondria dysfunction. Network analysis revealed that PDGFRA and IL6 were the top hub genes in treated NP cells. Furthermore, in irradiation-induced senescent NP cells, PDGFRA gene expression was significantly reduced compared to non-irradiated cells. However, rhPDGF-AB/BB treatment increased PDGFRA expression and mitigated the senescence progression through increased cell population in the S phase, reduced SA-β-Gal activity, and decreased expression of senescence related regulators including P21, P16, IL6, and NF-κB. Our findings reveal a novel anti-senescence role of PDGF in the IVD, making it a promising potential candidate to delay aging-induced IVD degeneration.

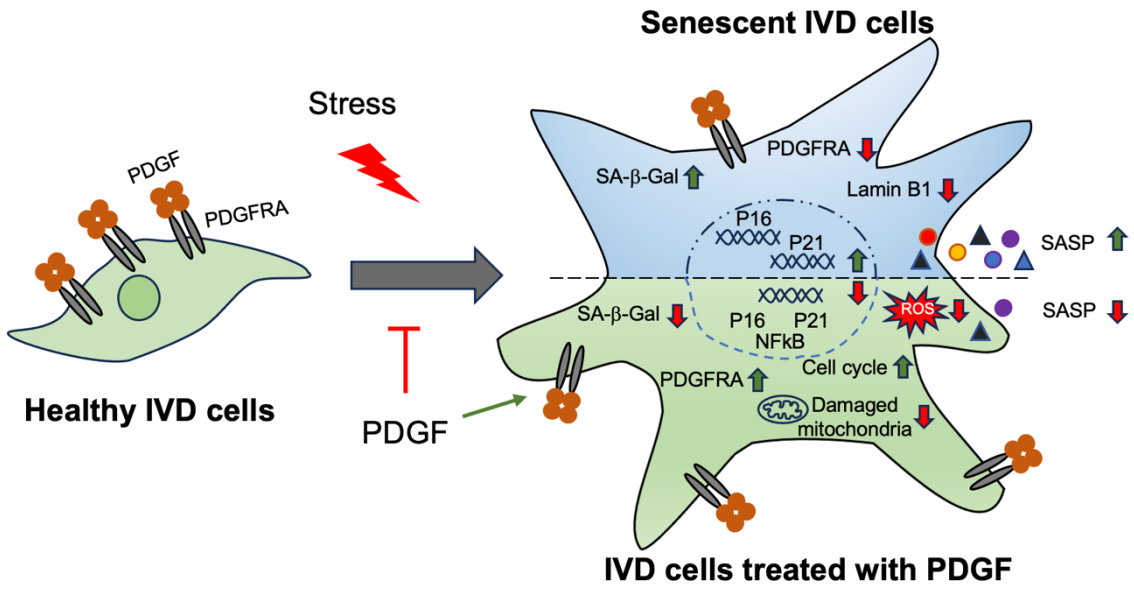


## Introduction

Low back pain (LBP), ranked as the first cause of years lived with disability, is a prevalent condition. Although the etiology of LBP is multifactorial, a major contributor of LBP is intervertebral disc (IVD) degeneration, which is increasing exponentially due to a growing aged population worldwide (Feng et al. 2016). Current treatments, such as medicine, physical therapy, and surgical excision of the herniated tissues, only temporally alleviate painful symptoms (Xin et al. 2022). In fact, patients often experience persistent LBP after surgery (Coronado et al. 2015). The fundamental cause of this is the inadequate knowledge of the underlying pathophysiology mechanisms leading to IVD degeneration. Therefore, it is crucial to understand the pathogenesis of IVD degeneration and develop novel therapeutic interventions to mitigate the degenerative processes.

The IVD consists of three compartments: the gelatinous nucleus pulposus (NP), fibrous annulus fibrosus (AF), and cartilaginous endplate (Sivan et al. 2014) . NP and AF tissues play distinct yet complementary roles in maintaining the spinal function. The NP has high content of proteoglycans and water, absorbing and distributing mechanical forces. In contrast, AF consists of multiple layers of concentric lamellae, which provides strength and stability to the disc and withstands compressive forces (Sivan et al. 2014; Pattappa et al. 2012). The NP plays a crucial role in the progression of IVD degeneration due to its susceptibility to significant structural and functional changes during aging and degeneration. Indeed, NP structural changes are easily detected through imaging techniques. Thus, because of its high-water content, MRI has made the NP the most visible indicator of disc degeneration in clinical practice. In contrast, degenerated alterations in the AF are more closely linked to pain and disability. As a result, effective therapeutic strategies for IVD degeneration should aim to restore the functionality of the entire disc unit.

Cellular senescence, triggered by normal cells in response to various intrinsic and extrinsic stressors, is a fundamental mechanism underlying age-related chronic diseases. Senescent cells are featured by irreversible growth arrest and acquire a senescent-associated secretory phenotype (SASP) and the secretion of pro-inflammatory cytokines, chemokines, and tissue-damaging proteases (Ngo et al. 2017). Activation of P53/P21 and P16 pathways play a critical role in regulating senescence (Reimann et al. 2024). In addition, NF-κB pathway is a major pathway involved in the expression of pro-inflammatory mediators in senescent cells (Salminen et al. 2012). Factors within the SASP can act in an autocrine manner to reinforce the senescent

state and induce senescence in neighboring cells via paracrine signaling (Kumari and Jat 2021). This mechanism elucidates the accumulation of senescent cells with aging and its associated detrimental effects. In the IVD, it has been well established that the number of senescent cells increases with aging and IVD degeneration (Veroutis et al. 2021; Gruber et al. 2007; Gruber et al. 2009), as demonstrated by increased senescence-associated β-galactosidase (SA-β-Gal) positive cells and decreased cell proliferation. Growing research also demonstrates that targeting cellular senescence holds promise in alleviating the progression of IVD degeneration. Long-term systemic or local clearance of senescent cells by senolytic drugs mitigated the age-related IVD degeneration in mice (Novais et al. 2021) and reduced the expression of pro-inflammatory cytokines and matrix proteases and restored IVD structure in an injury-induced IVD degeneration model in rats (Lim et al. 2022). Cherif et al. and Mannarino et al. demonstrated that in humans, senolytic drugs o-Vanillin (Mannarino et al. 2021) and RG-7112 (Cherif et al. 2020) attenuated NP cellular senescence, where a combination of these two senolytic drugs reduced the release of inflammatory factors and pain mediators in degenerated NP cells from low back pain patients (Mannarino et al. 2023).

PDGF is a major constituent of platelet rich plasma (PRP), which is widely used in the clinical setting for tissue regeneration and repair. It can be made of a homodimer of A, B, C, and D polypeptide chains, or an AB heterodimer (Chen et al. 2013; Heldin and Lennartsson 2013). Among these, PDGF-AB and -BB are the predominant forms in PRPs (Weibrich et al. 2002). Two types of PDGFR (PDGFRA and PDGFRB) were identified that differ in ligand-binding specificity. PDGFRA binds to all PDGF chains but D chain while PDGFRB only binds to B and D chains (Chen et al. 2013; Heldin and

Lennartsson 2013). Upon binding, PDGF-PDGFR network induces a cascade of phosphorylation in pathways including cell proliferation, migration, and survival (Contreras et al. 2021). We previously demonstrated that recombinant human PDGF-BB (rhPDGF-BB) inhibited cell apoptosis while promoting cell proliferation and matrix production in human IVD cells (Presciutti et al. 2014). Furthermore, when delivered via hydrogel, rhPDGF-BB successfully inhibited IVD degeneration and restored IVD biomechanical function in a rabbit preclinical model of puncture-induced IVD degeneration (Paglia et al. 2016). In the current study, we hypothesize that PDGF-AB and -BB mitigated IVD degenerating through targeting cellular senescence. To test it, aged, degenerated human IVD cells were treated with rhPDGF-AB or -BB and transcriptome profiling was performed on treated NP and AF cells. We found similar but distinct responses to the treatment between NP and AF cells. In NP cells, PDGF-AB and -BB treatment upregulated the expression of PDGFRA and genes involved in cell cycle progression while downregulating the expression of genes related to ROS production, oxidative stress, and mitochondrial function. The alterations in these pathways indicated that the senescent phenotype was alleviated in human degenerated IVD cells treated with PDGF-AB/BB. Furthermore, in human senescent NP cells induced by irradiation, PDGFRA was significantly reduced while PDGF-AB/BB treatment mitigated the progression of senescence through increased cell cycle progression and reduced SA-β-Gal staining and the expression of P21, P16, NF-κB, and IL6.

## Methods

### 2.1 Sample collection and cell extraction

This study was conducted in accordance with the ethical principles outlined in the Declaration of Helsinki. All experiments and procedures were reviewed and approved by the institutional review board of Emory University (IRB #00099028) approval. Human degenerated NP and AF tissues (Grade IV or V on Pfirrman grade; 64.6 ±8.5 years old)) were obtained as the surgical waste from donors with disc herniation, with each donor providing written informed consent. Healthy NP and AF cells (23.0 ±3.7 years old) were gifted by Professor Lisbet Haglund from McGill University (Tissue Biobank #2019-4896). The donor information was listed in **Table 1**. NP and AF cells were extracted as previously described (Zhang et al. 2024). Isolated cells were expanded in growth media containing low glucose DMEM, 10% FBS, 1X antibiotic-antimycotic (Thermofisher Scientific, 15240062), and 50 µg/ml L-Ascorbic acid 2-phosphate (Sigma, A8960). Cells were grown at 37°C under 5% $CO_2$ and 20% $O_2$. To minimize the variability between experiments that may be caused by changes in cell behavior with each passage, cells of passage 3 were used for each experiment.

### 2.2 PDGF treatment in human intervertebral disc cells

To synchronize cells and enhance the sensitivity of cells to PDGF stimulation, degenerated NP (n =5/each group) and AF cells (n =6/each group) were serum-deprived in low glucose media containing 0.2% FBS for 1 day. Cells were then treated with recombinant human PDGF-AB (40ng/ml; PeproTech, 10770584) or -BB (20ng/ml; PeproTech, 10771918) for 5 days.

### 2.3 RNA-sequencing

Total RNA was isolated with TRIzol (ThermoFisher Scientific, 15596018) and purified using miRNeasy kit (Qiagen, 217084). Genomic DNA contamination was eliminated through on-column DNase digestion. The concentration and quality of RNA were determined using Nanodrop and RNA integrity was assessed by Agilent 2200 Bioanalyzer. RNA samples (NP: n = 5, AF: n = 6) with RIN > 7 were shipped in dry ice to Novogene for RNA-sequencing, which was carried out using NovaSeq 6000 (Novogene Corporation Inc). Libraries were constructed from 0.2μg RNA using TruSeq Stranded Total RNA Sample Prep Kit (Illumina). Quality control was performed for distribution of sequencing error rate and GC content and data filtering was performed to remove the low-quality reads and reads containing adapters. The resulting sequences were uploaded into the NCBI Sequence Read Archive (SRA) database (PRJNA1150962). The clean reads were mapped to human reference genome sequence using DNASTAR.

**2.4 Differential gene expression analysis of RNA-seq data**

Unnormalized raw counts exported from DNASTAR were used for pairwise gene expression comparison between untreated and PDGF-AB/BB samples. Differential expression genes (DEGs) were identified using DESeq2 package in R and DEGs with fold change greater than 1.5 and adjusted p value less than 0.05 were considered statistically significant. Heatmap and volcano plots and principal component analysis were performed to visualize the DEGs between untreated and PDGF-AB/BB samples.

**2.5 Pathway enrichment analysis**

To identify the biological process that DEGs were enriched, Gene ontology (GO) analysis was performed using upregulated and downregulated DEGs separately in R.

The significantly enriched GO terms were visualized by dot plot analysis. GeneRatio in X-axis was calculated by the ratio of gene counts enriched in a particular GO term to all the gene counts annotated in the GO term.

Gene Set Enrichment Analysis (GSEA) was performed on all the genes to determine whether a predefined set of genes is significantly enriched in untreated or PDGF-BB samples. GSEA was conducted based on KEGG (Kyoto Encyclopedia of Genes and Genomes) database using clusterProfiler package in R (Wu et al. 2021) and a gene set was considered significantly enriched when the false discovery rate (FDR) was less than 0.05. Enrichment score (ES) was calculated to reflect the degree to which a gene set is overrepresented in our dataset, which was ranked based on fold change. Normalized enrichment score (NES) is the ES normalized to the gene set size.

**2.6 Protein-protein interaction network analysis**

The interactions among DEGs were performed using the Search Tool for the Retrieval of Interacting Genes (STRING) database (v12.0) with an interaction score greater than 0.4. Discrete proteins were removed, and the node files were exported and visualized in Cytospace (v3.10.0). To identify essential nodes in the interaction network, the betweenness centrality among the nodes was calculated using CytoNCA plugin (v2.1.6) in Cytospace (Tang et al. 2015) and the top 10 hub nodes were identified using CyoHubba plugin (v0.1) (Chin et al. 2014).

**2.7 Cellular senescence induction by irradiation**

To induce cellular senescence, cells were seeded in 6-well plate at a density of 5 X $10^4$ cells/ml and cultured in low glucose DMEM supplemented with 10% FBS, 1X antibiotic-

antimycotic (Thermofisher Scientific, 15240062), and 50 μg/ml L-Ascorbic acid 2-phosphate (Sigma, A8960). After 48 hours of culture, growth media was removed, and cells were washed with 1 X PBS once. To minimize the interference of culture media with the irradiation process, 500ul PBS was added before irradiation. Healthy NP and AF cells (n=4/each group) were exposed to a single dose of 5 Gy, 10 Gy, or 15 Gy of X-ray in a CellRad benchtop X-ray irradiator (Precision X-Ray) at a rate of 2.6 Gy/min. The irradiation doses and rate were selected based on prior studies (Ungvari et al. 2013; Zhong et al. 2022) and optimized to effectively induce senescence associated changes in human IVD cells without triggering excessive cells death, which is often observed at higher irradiation doses. After irradiation, cells were immediately incubated with growth media. Cells exposed to 10 Gy of irradiation showed the most pronounced senescent phenotype on day 10 and were used for further experiments. For treatment experiments, cells were exposed to 10 Gy of X-ray and treated with PDGF-AB/BB (20ng/ml) immediately after irradiation for 10 days. The culture media was changed every other day.

### 2.8 Senescence-associated β-galactosidase (SA-β-Gal) staining

SA-β-Gal staining was performed according to the manufacturer's protocol (Cell Signaling Technology, #9860). In brief, cells cultured in 6-well plates were washed in PBS and fixed with 1X fixative solution for 10 min. 1 ml of β-Gal staining solution (containing 1 mg/ml X-Gal) was added and the cells were incubated at 37 °C in the absence of $CO_2$ overnight. Cells were washed in PBS and observed under bright-field microscope (ECHO Revolve).

## 2.9 Immunocytochemistry

Cells cultured on glass coverslips were washed in 1 X PBS and fixed in 4% (v/v) formaldehyde for 10 min. After washing in 1 X PBS, cells were premetallized in PBS with 0.1% Trition X-100 for 15 min. Non-specific binding sites were blocked in 0.1% Tween-20/PBS with 1% bovine serum album for 30 min, followed by incubating with primary antibodies against P21 (1:500, Cell Signaling Technology, #2947), P16 (1:500, Cell Signaling Technology, #80772), or Lamin B1 (1:500, Cell Signaling Technology, #68591S ). After overnight incubation at 4 °C, the cells were washed and incubated with the corresponding host-specific secondary antibodies goat anti mouse Alex Fluor 488 (1:1000, #ab150113), or goat anti rabbit Alex Fluro 647 (1:1000, #ab150079) for 1 hour. Cells were counterstained and mounted with mounting medium with DAPI (Abcam, #ab104139) and visualized using an Olympus BX63 automated fluorescence microscope.

## 2.10 Quantitative real-time PCR assays

Total RNA was extracted from cells collected in TRIzol reagent (Thermofisher Scientific, #15596018) and RNA quality was measured using NanoDrop-1000 spectrophotometer (Thermofisher Scientific, #ND-2000). 1μg of RNA was reverse transcribed using Verso cDNA synthesis kit (Thermofisher Scientific, #AB-1453B). Quantification of mRNA expression was determined by SYBR-based real-time PCR using PowerUp SYBR Green Master Mix (Applied Biosystems, #A25742). PCR primer sequences were listed in **Table 2.** Values were normalized to *ACTB*. mRNA levels were presented as fold change compared to untreated cells according to the $2^{-\Delta\Delta CT}$ method.

### 2.11 Immunoblotting

Whole-cell protein extraction and immunoblotting analysis were performed as previously described (Zhang et al. 2024). Briefly, cells were lysed using RIPA lysis buffer with 1 X protease and phosphatase inhibitor (ThermoFisher Scientific, #PI78440). Protein concentration was determined using Pierce BCA protein assay kit (ThermoFisher Scientific, #23225) and 20 μg of cell lysate from each sample was used to determine the protein expression of P21 (1:2000, Cell Signaling Technology, #2947) and NF-kB (1:2000, Cell Signaling Technology, #8242S). All proteins were normalized to b-actin (1:2000, Cell Signaling Technology, #5125S).

### 2.12 Statistics

One-way analysis of variance (ANOVA) testing was performed to assess the effects of treatment on NP and AF cells with subsequent Dunnett post hoc testing. To analyze the effects of ionizing radiation on the expression of senescence markers in cells, t-test was utilized. The statistical analyses were performed using GraphPad Prism9. A p-value $< 0.05$ was considered statistically significant.

## 3 Results

### 3.1 Transcriptomics of AF and NP cells in response to PDGF-AB/BB

Bulk RNA sequencing was performed to investigate the global changes in gene expression of degenerated AF and NP cells in response to rhPDGF-AB/BB treatment. Principal component analysis (PCA) on all detected genes revealed distinct clusters between untreated and rhPDGF-AB/BB treated samples while clusters of rhPDGF-AB and rhPDGF-BB treated samples were overlapping (**Supplementary figure 1**). As

shown in volcano plots, differential expression analysis (|FC|>1.5 and FDR < 0.05) revealed 880 downregulated and 740 upregulated genes in AF cells treated with rhPDGF-AB and 996 downregulated and 821 upregulated genes induced by rhPDGF-BB treatment after 5 days exposure (**Figure 1A**). In contrast, NP cells had 563 downregulated and 423 upregulated genes in rhPDGF-AB treated group and 409 downregulated and 404 upregulated genes in rhPDGF-BB treated group. The top differentially expressed genes (DEGs) were annotated according to FDR and most of these genes exhibited similarity between treatment groups in both AF and NP cells (**Figure 1A+B**). Furthermore, a heat map visualizing the top 50 DEGs by fold change revealed variability among donors while demonstrating an overall consistent response to rhPDGF-AB/BB treatment across the samples (**Figure 1C+D**). Tissue-specific changes were observed in AF and NP cells when treated with rhPDGF-AB/BB. For example, *SLC26A4* (Pendrin) and *CA2*, regulators of the process of transporting and producing bicarbonate, are involved in the homeostatic control of pH in various type of cells (Vince and Reithmeier 1998; Silagi et al. 2018) and their expression was upregulated in NP cells when treated with rhPDGF-AB/BB (**Figure 1D**). *MAMDC2* and *COL21A1*, involved in extracellular matrix organization (Chou and Li 2002; Mavillard et al. 2023) , were also upregulated in NP cells while *WISP2* (Ruiz-Fernández et al. 2022) and *RARRES2* (Liu-Chittenden et al. 2017), modulators of the induction of inflammatory mediators and immune response, were downregulated after treatment. In contrast, in addition to the commonly upregulated *CA2, MDMC2* and *RARRES2*, AF cells showed alterations in genes involved in mechanical stress, pain sensation, and angiogenesis, such as *CSRP3* (Rashid et al. 2015), *PI16* (Singhmar et al. 2020), *EFEMP1* (Song et al.

2011) and *SLC26A4-AS1* (Li et al. 2021) (**Figure 1C**). Notably, *PRELP*, potentially associated with Hutchinson-Gilford progeria (Lewis 2003), was also downregulated in rhPDGF-AB/BB treated AF cells (**Figure 1A**).

### 3.2 Functional analysis of AF cells treated with PDGF-AB/BB

To investigate the enriched biological processes (BP) induced by rhPDGF-AB/BB treatment in AF cells, gene ontology (GO) analysis was performed using upregulated and downregulated DEGs separately. As expected, the biological processes between rhPDGF-AB and -BB treated samples were mostly overlapping (**Figure 2A+B**). In AF cells, upregulated DEGs were significantly enriched in biological processes including regulation of cell cycle and chromosome segregation. Furthermore, AF cells demonstrated upregulated pathways including mesenchymal cell differentiation and response to oxygen levels and downregulated pathways including response to ROS and oxidative stress (**Figure 2A**). Moreover, the treatment downregulated groups of genes related to neurogenesis and response to mechanical stimulus (**Figure 2B**). In line with the results of GO analysis, GSEA analysis revealed an overrepresentation of cell cycle pathway in rhPDGF-AB/BB treated cells (**Figure 2C**). Additionally, the ErbB signaling pathway, proteasome pathway, and cytosolic DNA-sensing pathway were enriched, suggesting that PDGF-AB/BB treatment promoted cell growth, protein turnover, and maintenance of cellular homeostasis. The leading-edge genes that contributed most significantly to these pathways include *CCNB1, CCND1, AREG, PSMB9, TREX1,* and *POLR3A*, as shown in **Figure 2D.** Protein-protein interaction (PPI) network was employed to further investigate the potential connectivity of DEGs between untreated and treated groups using the STRING and Cytoscape softwares (**Figure 2E**). PPI

analysis revealed that the hub genes in rhPDGF-AB treated samples were associated with inflammation (*CCN2, CSF3, OASL and SOCS1*), macrophage function (*CSF1R*), neurogenesis (NGF, APOE), and angiogenesis (PTGS2). In rhPDGF-BB treated AF cells, *PXDNL,* a member of the peroxidase enzyme family and participating in scavenging ROS interacted with *IL18*, an activator of NF-kB signaling. Additionally, *CD36*, involved in angiogenesis, was among the top 10 hub genes. Taken together, these findings suggest that PDGF treatment promoted cell mitogenesis while inhibiting oxidative stress, inflammation, neurogenesis, and response to mechanical stimulus.

### 3.3 Functional analysis of NP cells treated with PDGF-AB/BB

GO analysis revealed similar yet distinct responses to rhPDGF-AB/BB treatment between NP and AF cells. In NP cells**,** rhPDGF-AB and -BB treatment upregulated groups of genes related to cartilage development, cell-matrix adhesion, Wnt signaling pathway, and response to decreased oxygen levels, which were all important to maintaining NP phenotype (**Figure 3A**). Downregulated DEGs were enriched in GO terms associated with fatty acid metabolism, cellular respiration, mitochondrial function, and reactive oxygen species production (**Figure 3B**), suggesting alterations in cellular metabolism and oxidative stress. Gene set enrichment analysis (GSEA) on the entire transcriptomics also revealed that Wnt signaling pathway and neuroactive ligand-receptor interaction were upregulated while the pathways related to oxidative phosphorylation and ribosome were downregulated in rhPDGF-BB treated NP cells (**Figure 3C**). The core enrichment genes associated with these pathways were visualized in a chord diagram (**Figure 3D**). Specifically, the leading-edge DEGs enriched in Wnt signaling pathway include *WNT7B, WNT5A, NKD1*, and *SFRP1* and

oxidative phosphorylation pathway showed enrichment in *NDUFB7, NDUFA11, COX5B*, and *CYC1*.

To better understand the regulatory mechanisms of PDGF-AB/BB in degenerated NP cells, DEGs between untreated and treated groups were used to construct PPI networks. The network of the top 10 hub nodes based on betweenness was demonstrated in **Figure 3E** and it revealed the strong correlation between *PDGFRA (*PDGF receptor alpha) and *IL6, MDM2*, *MDM2*, *CCND1, PIK3R1, NOP53, FN1,* and *IDH2*. The enrichment of hub gene *IDH2*, which plays a role in generating NADPH within mitochondria, further validated the alterations in oxidative phosphorylation pathway and subsequent ROS production, as indicated by GSEA and GO analysis in rhPDGF-AB/BB treated NP cells. *MDM2* (a negative regulator of P53) and predicted *NOP53* (a regulator of P53 binding activity) suggested that PDGF-BB interfered with P53 signaling pathway. The interaction between these genes and inflammatory cytokine *IL6* indicated a potential involvement of PDGF-AB/BB in cellular senescence. The gene expression of top hub genes PDGFRA and IL6 was further verified in both NP (**Figure 3F**) and AF (**Figure 3G**) cells by qPCR. PDGF-AB/BB increased the gene expression of PDGFRA in only NP cells and reduced the IL6 gene expression in both type of cells. Interestingly, the protein expression of PDGFRA was decreased in treated NP and AF cells compared to untreated groups (**Supplementary figure 1**). The discrepancy in changes between gene and protein expression levels reflects the complexity in the dynamic regulation of PDGFRA (**Supplementary figure 1)**. Taken together, NP and AF cells responded differently to PDGF-AB/BB treatment, but both cell types showed a positive regulation of

cell cycle and inhibited inflammation, response to ROS, oxidative stress, and mitochondrial dysfunction, indicating a role of PDGF-AB/BB in IVD cell senescence.

### 3.4 Induction of NP cellular senescence through X-ray radiation

To test our hypothesis that PDGF-AB/BB provides protection against the progression of cellular senescence in the IVD, we first created a cellular senescence model using X-ray radiation. The healthy NP cells were exposed to 5, 10 and 15 Gy of irradiation and cultured for 7-10 days to develop senescent phenotype. SA-β-gal staining was performed to detect senescent cells. We found that non-irradiated, proliferating NP cells showed elongated, spindle-shaped morphology and faint SA-β-gal staining at day 7 (**Figure 4A**). In contrast, cells exposed to 5 and 10 Gy of irradiation developed characteristics of a senescent cell phenotype — enlarged cell size, low cell number, and a higher percentage of SA-β-gal positive cells. However, cells exposed to 15 Gy of radiation underwent significant cell death, showing negligible SA-β-gal staining. As a result, we excluded the 15 Gy dosage group in subsequent studies. To quantify cell growth, MTT assay was performed, which revealed reduced cell proliferation under 5 and 10 Gy of irradiation compared to the non-irradiated group (**Figure 4B**). Furthermore, we examined the expression of senescence related markers — Lamin B1, P21 and P16. Lamin B1 is a structural component of the nucleus, and its loss is a senescence-associated biomarker (39). Non-irradiated cells displayed nuclear Lamin B1 expression while its expression was lost in healthy NP cells exposed to 5 and 10 Gy of irradiation for 7 days (**Figure4C**). Meanwhile, nuclear localization of P21 (**Figure 4C**) and P16 (**Figure 4D**) was observed in irradiated cells, with little immunopositivity in non-irradiated cells at day 7. However, the transcripts of *P21* and *P16* were not significantly

decreased until day 10 (**Figure 4E+F**). Caspase 3 (*CASP3*) gene expression was reduced at both timepoints, suggesting that the irradiated cells were resistant to apoptosis. Furthermore, the gene expression of *PDGFRA* was significantly decreased in cells under 10 Gy of irradiation at day 10. Taken together, when exposed to irradiation for 10 days, healthy human NP cells developed senescent phenotype, accompanied with decreased PDGFRA expression.

### 3.5 PDGF-AB/BB inhibited senescent phenotype in NP and AF cells

To investigate the protective effects of PDGF-AB/BB against cell senescence in the IVD, healthy human NP and AF cells were exposed to 10Gy of irradiation, followed by immediate treatment with 20 ng/ml rhPDGF-AB/BB for 10 days. We first examined the cell cycle progression using DAPI stained cells and found that rhPDGF-BB significantly increased the percentage of cell population in the S phase in irradiated NP (**Figure 5A-B**) and AF (**Figure 5C-D**) cells at day 10. In rhPDGF-AB treated cells, the percentage of cell population in the S phase was increased in AF cells, but not significantly in NP cells. These findings suggested that PDGF-AB/BB rescued IVD cells from cell cycle arrest in irradiation induced senescent cells. Additionally, SA-β-gal staining demonstrated an increase in the number of senescent cells after irradiation at day 10, whereas a decrease was examined in rhPDGF-AB/BB treated NP and AF cells (**Figure 5E**).

At day 10, we analyzed the expression of *PDGFRA* and key senescence regulators of cell cycle inhibitors *P21* and *P16*, *CASP3*, and SASP mediator *IL6.* The treatment of rhPDGF-BB to irradiated NP cells significantly increased the gene expression of *PDGFRA* and decreased the gene expression of *P21*, *P16*, and *IL6*, while playing no effect in the gene expression of *CASP3* **(Figure 6A)**. Comparably, the treatment of

rhPDGF-AB to irradiated NP cells significantly decreased the gene expression of *P21* and *IL6* and played no effect on the gene expression of *PDGFRA*, *P16*, and *CASP3* **(Figure 6A)**. In AF cells, the results show that the treatment of rhPDGF-BB and rhPDGF-AB reduced the gene expression of *P21* as those of NP cells **(Figure 6B)**. However, the treatment of either rhPDGF-BB or rhPDGF-AB had no effect in the gene expression of other genes examined **(Figure 6B)**. The lack of change in the gene expression of *PDGFRA* from the treatment of either rhPDGF-BB or rhPDGF-AB suggested that PDGF-BB reduced senescent phenotype through other receptors in AF cells.

Furthermore, compared to irradiation only group, the protein levels of P21 and NF-κB, a major regulator stimulating SASP, were inhibited in rhPDGF-BB treated NP cells (**Figure 6C**). In irradiated AF cells, the protein expression of P21 was significantly reduced by rhPDGF-BB treatment. The expression of NF-kB showed a decreasing trend in rhPDGF-BB treated cells. rhPDGF-AB had no effects on the protein expression of P21 and NF-kB. Overall, PDGF-BB mitigated the progression of senescent phenotype in both human NP and AF cells.

## Discussion

The current study has shown for the first time that PDGF-AB and -BB treatment not only alleviated the senescent phenotype, but also suppressed the progression of cellular senescence in the IVD. Specifically, in aged, degenerated human NP and AF cells, PDGF-AB/BB treatment suppressed the ROS accumulation, mitochondrial dysfunction, and the resultant oxidative stress, while stimulating cell cycle progression. In the NP, PDGFRA was among the top hub genes that showed strong interaction with other

genes. Moreover, its expression was significantly reduced in irradiation induced senescent cells. Importantly, immediate PDGF-BB treatment after irradiation promoted the expression of *PDGFRA* and mitigated senescence associated phenotype in healthy IVD cells. This novel function of PDGF-BB/PDGFRA signaling is likely linked to their ability to inhibit NF-κB, P16, and P21 pathways in NP cells. In contrast, while PDGF treatment alleviated the senescent phenotype in AF cells, it also induced changes in pathways such as response to mechanical stimuli and neurogenesis, which were distinct from those in NP cells. This indicates that the treatment enhanced IVD functionality through different mechanisms within the two compartments. Senescence is a key contributor to the onset and the progression of IVD degeneration (Silwal et al. 2023). It can occur naturally with aging or can be triggered by growth factor deficiency, radiation, DNA damage, oxidative stress, and inflammatory stimuli (Wang et al. 2016)(Huang et al. 2022). Senescent cells exit the cell cycle and cannot divide; their accumulation reduces the IVD's ability to generate new cells to replace apoptotic or necrotic cells. It has been well established that increased number of senescent cells was positively correlated with the IVD aging and the severity of degeneration while negatively correlated with the percentage of proliferating cells in human NP and AF tissues (Gruber et al. 2009; Veroutis et al. 2021; Gruber et al. 2007). Since PDGF is a mitogenic growth factor and promotes cell proliferation in various cell types (Contreras et al. 2021; García-Olivas et al. 2007; Martin-Garrido et al. 2013), it is intriguing to explore whether PDGF-AB/BB could mitigate or prevent against the cellular senescence in IVDs. We observed groups of upregulated genes regulating cell cycle progression and cell proliferation in PDGF-AB/BB treated NP cells. AF cells also had an upregulation

of chromosome segregation and mitotic nuclear division pathways, suggesting that these cells were actively proliferating. Cell cycle progression is controlled by cyclins, and the expression of cyclin D1 and B1, regulators of the G1/S and G2/M phase transition respectively, was increased in degenerated NP cells after PDGF-AB/BB treatment. Transcriptomic analysis also revealed that increased cyclin D1 was among the top hub nodes, tightly regulated by PDGF-AB and BB. In addition, cell cycle analysis confirmed that PDGF-AB/BB induced the transition from G1 to S1 phase in senescent IVD cells. Our data suggested that PDGF treatment led to an increase in the proliferation of senescent IVD cells in the S phase likely through cyclin D1 and B1. These findings were in accordance with previous studies showing that PDGF stimulated cell proliferation and cyclin D1 expression in rat mesangial cells (Hida et al. 2003), rat adventitial fibroblasts (Chen et al. 2023), and human vascular smooth muscle cells (Martin-Garrido et al. 2013).

The antisenescence of PDGF has been demonstrated in several studies. For example, PDGF-BB decreased SA-β-gal positive cells and the expression of P53 and P21 while enhancing proliferative potential in senescent human dermal fibroblasts (Bae et al. 2016) and mesenchymal stem cells (MSCs) derived from immune thrombocytopenia patients (Zhang et al. 2016). PDGF exerts its function by binding to its receptors, thereby triggering a cascade of intracellular signaling events, such as cell proliferation and survival. The PDGF-PDGFRA signaling is often suppressed in premature aged or senescent cells (Tan et al. 2018; Pan et al. 2019; Mori et al. 1993), suggesting that PDGF signaling dysfunction might be involved in senescence or aging. Notably, our transcriptome data has shown that both PDGF-AB and -BB induced the expression of

*PDGFRA* in aged, degenerated NP cells. This autoregulatory loop caused IVD cells to become more sensitive to PDGF treatment and augmented the signaling cascades triggered by PDGF binding, including senescence-associated P21, P16, P53, and NF-κB pathways. In line with this thought, PPI analysis revealed that *PDGFRA* closely interacted with upregulated *MDM2*, a negative regulator of P53. NF-κB signaling is a major signaling pathway that is involved in inflamm-aging (Songkiatisak et al. 2022) and induces the onset of SASP (Salminen et al. 2012), such as IL6, IL8, and CXCL1. In our study, irradiation in NP cells led to decreased *PDGFRA* expression, which impaired the activity of PDGF/PDGRFA signaling. However, PDGF-BB treatment promoted the expression of *PDGFRA* and decreased the expression of *P21, P16,* and *IL6* in senescent NP cells, likely by inhibiting NF-κB signaling. In fact, it has been shown that NF-kB signaling was elevated in mouse IVDs exposed to a single 20 Gy dose of irradiation in an ex vivo culture model (Liu et al. 2020). These findings support the idea that PDGF treatment could stimulate the expression of *PDGFRA* and mitigated the progression of senescent phenotype in healthy IVD cells. Interestingly, while mRNA level was increased in PDGF treated NP cells, its protein level was decreased, highlighting the complexity in PDGF receptor dynamics. Upon binding with PDGF ligands, PDGFRA is known to undergo rapid internalization and degradation, a mechanism that prevents overstimulation of the signaling pathway (Rogers and Fantauzzo 2020). The upregulated gene expression probably compensates for this degradation and supports continued activation of PDGFRA signaling activation, emphasizing its crucial role in response to the PDGF treatment. Further studies using

preclinical animal models to validify the protectiveness of PDGF against the onset or progression of senescence in the IVD will offer more robust evidence.

Degenerated IVD cells experienced an imbalance between ROS accumulation and antioxidant capacity, leading to oxidative stress, which is involved in cellular senescence (Feng et al. 2017). Mitochondrion is the primary location of intracellular ROS production and its dysfunction in degenerated IVD cells causes electron leakage, resulting in the formation of superoxide radicals (Wang et al. 2022). PDGF-AB/BB treatment suppressed the activity of damaged mitochondria, leading to decreased ROS and oxidative stress in degenerated NP and AF cells, as indicated by GO BP analysis. Consistently, GSEA revealed the underrepresentation of oxidative phosphorylation in treated NP cells. The downregulation of genes related to mitochondria activity and oxidative phosphorylation may be indicative of a shift in metabolic pathways, leading cells to potentially prioritize alterative pathways such as glycolysis. Indeed, PDGF treatment upregulated groups of genes involved in response to decreased oxygen levels, suggesting that the treatment activated cellular mechanisms involving in sensing and adapting to low oxygen conditions. In line with this idea, it has been demonstrated that hypoxia-inducible factor 1$\alpha$ is highly expressed in healthy NP cells to suppress oxidative phosphorylation and enhanced glycolysis, allowing cells to adjust to a hypoxia microenvironment (Song et al. 2024; Silagi et al. 2021). Conversely, degenerated NP cells show an opposite metabolic pattern (Song et al. 2024; Silagi et al. 2021).

Besides the anti-senescence, NP and AF cells responded differently to PDGF-AB/BB treatment. AF cells were more responsive to the treatment with twice as many DEGs as NP cells. The difference in tissue architecture and cellular contents between NP and AF

contributes to their specialized functions (Kudelko et al. 2021). The multiple layers of concentric lamellae in the AF enables it to withstand circumferential loads while this highly organized structure was disrupted with aging and degeneration (Dittmar et al. 2016). In addition, damage to the AF has the potential to stimulate neovascularization and nerve ingrowth, provoking an inflammatory response and contributing to low back pain. PDGF-AB/BB treatment downregulated groups of genes related to neurogenesis and response to mechanical stimulus in AF cells while downregulated genes in the NP were more associated with metabolic pathways, providing evidence that the treatment enhanced IVD functionality in different aspects between the two compartments.

Senescence as a central hallmark of aging can be induced by several factors (Silwal et al. 2023). One limitation of this study is that we did not examine the effects of PDGF-AB/BB treatment on senescence using other senescence models. In addition, our findings were obtained in vitro experiments, so caution is needed when interpreting our data. Our future work will focus on establishing an appropriate experimental animal model to study the functions of PDGF on cellular senescence.

In this study, we demonstrated a novel function of PDGF in human NP and AF cells. PDGF-AB/BB treatment alleviated oxidative stress and mitochondria dysfunction while stimulating cell cycle progression in degenerated IVD cells. In addition, the treatment mitigated the progression of senescence in healthy NP and AF cells following irradiation. These findings suggest that PDGF-AB/BB may serve as a promising potential candidate for IVD degeneration by targeting cellular senescence.

**Human ethics and consent to participate:**

This study was conducted in accordance with the ethical principles outlined in the Declaration of Helsinki. All experiments and procedures were reviewed and approved by the Institutional Review Board (IRB #00099028) of Emory University for all experimental procedures. Human tissue samples were collected after obtaining familial consent.

**Funding statement**

Funded by NIH-R01AR076427 to HD, and the Department of Orthopaedics at Emory University School of Medicine. The authors also express their gratitude to Mr. Jack McKee for his gift to support our departmental spine research.

**Acknowledgement**

The authors thank Gilbert Gu for his assistance in correcting the grammar in the manuscript.

**Conflict of interest:**

The authors have no conflict of interest associated with this work.

**Authors' contributions:**

CZ designed and conducted the study, analyzed and interpreted the data, and drafted the manuscript. TF and MDH reviewed and revised the manuscript. SS assisted in data collection. SY provided diseased IVD tissues and reviewed the manuscript. LH provided healthy IVD cells and revised the manuscript. HD designed the study and interpreted

the data. All authors have reviewed the manuscript and provided their consent for publication.

**Availability of data and materials:**

The datasets and code used and analyzed during the current study are available from the corresponding author on reasonable request.

**Figure legends**

**Figure 1. Transcriptomics of AF and NP cells in response to PDGF-AB/BB treatment. A + B**) Volcano plots showing the differentially expressed genes (DEGs) in AF (**A**) and NP (**B**) cells treated with rhPDGF-AB/BB for 5 days (cutoff: |FC| > 1.5 and FDR < 0.05). DEGs were annotated in the plot according to FDR. **C+D)** Heatmap plots showing the top 50 DEGs in rhPDGF-AB/BB treated AF (**C**) and NP (**D**) cells based on fold change. NP: n = 5 samples. AF: n = 6 samples.

**Figure 2. Functional analysis of AF cells treated with PDGF-AB/BB. A + B)** Gene ontology (GO) analysis for biological process using upregulated (**A**) and downregulated (**B**) DEGs in AF cells. Y-axis label represents GO terms, and x-axis represents geneRatio (geneRatio refers to the proportion of genes that are annotated in specific GO term within all the input genes). The size of bubble represents the gene counts enriched in a particular GO term and the color indicates the FDR of GO terms. **C)** Gene set enrichment analysis (GSEA) on the entire transcriptome profile demonstrated an

upregulation of cell cycle, cytosolic DNA-sensing pathway, ErbB signaling pathway, and proteasome and a downregulation of drug metabolism-cytochrome P450 pathway in rhPDGF-BB treated NP cells. **D**) The leading-edge genes associated with these pathways were shown using a chord diagram. **E)** Protein-protein interaction network using DEGs was constructed in STRING and visualized in Cytospace.

**Figure 3. Functional analysis of NP cells treated with PDGF-AB/BB. A + B)** Gene ontology (GO) analysis for biological process using upregulated **(A)** and downregulated **(B)** DEGs in NP cells. Y-axis label represents GO terms, and x-axis represents geneRatio (geneRatio refers to the proportion of genes that are annotated in specific GO term within all the input genes). The size of bubble represents the gene counts enriched in a particular GO term and the color indicates the FDR of GO terms. **C)** Gene set enrichment analysis (GSEA) on the entire transcriptome profile demonstrated an upregulation of Wnt signaling pathway and a downregulation of oxidative phosphorylation and ribosome in rhPDGF-BB treated NP cells. **D)** The leading-edge genes associated with these pathways were shown using a chord diagram. **E)** Protein-protein interaction network using DEGs was constructed in STRING and visualized in Cytospace. **F+G)** The changes in the gene expression of PDGFRA and IL6 were verified in NP **(F)** and AF **(G)** cells treated with rhPDGF-AB (40ng/ml) or -BB (20ng/ml) for 5 days. *$p< 0.05$. **$p< 0.01$. ***$p< 0.001$.

**Figure 4. Cellular senescence induction by irradiation**. **A)** SA-b-gal staining in healthy NP cells under different doses of irradiation at day 7. Images were captured under 10X magnification using Echo microscope. ROI: region of interest. **B)** MTT assay showed decreased cell proliferation after irradiation at day 7. **C**) Immunocytochemistry

staining on Lamin B1 and P21 in irradiated cells at day 7. **D)** Quantification of P21 positive cells. **E**) Immunocytochemistry staining on P16 in irradiated cells at day 7. **F)** Quantification of P16 positive cells. **G)** Changes in the gene expression levels of *P21, P16,* and *CASP3* in NP cells under 10 Gy of irradiation compared to the non-irradiated group at day 7 and 10 timepoints. **H**) The gene expression of *PDGFRA* was reduced under 10 Gy of irradiation compared to the non-irradiated group at day 10. *$p < 0.05$. **$p < 0.01$. ***$p < 0.001$. ****$p < 0.0001$.

**Figure 5. PDGF-AB/BB treatment inhibited the progression of senescence in healthy NP and AF cells exposed to irradiation. A-F)** Cell cycle analysis by DAPI staining in irradiated healthy NP **(A-C)** and AF **(D-F)** cells treated with rhPDGF-AB(40ng/ml) or BB (20ng/ml) for 10days. The upper panel shows the data obtained from NP cells, and lower panel shows the data from AF cells. Representative graphs **(A+D)** showing the changes in cell cycle progression in NP and AF cells after treatment. **B+E)** Quantification of cell cycle analysis showed the cell percentage in each phase. Two-way ANOVA with Dunnett post hoc testing was performed. n = 4 each group. **C+ F)** The cell percentage in the S phase was shown to examine the effects of treatment on cell proliferation. One-way ANOVA with Dunnett post hoc testing was performed. n = 4 each group. **G)** SA-b-gal staining in irradiated healthy NP (upper panel) and AF cells (lower panel) showing the reduced SA-b-gal positive cells in after treatment. Images were captured under 10X magnification using Echo microscope. ROI: region of interest. The data is presented as mean with SD. *$p < 0.05$. **$p < 0.01$.

**Figure 6. PDGF-AB/BB treatment suppressed the expression of senescence**

**associated regulators**. **A-B)** Changes in the gene expression of *PDGFRA*, *P21, P16, CASP3,* and *IL6* in irradiated NP (**A)** and AF (**B)** cells treated with rhPDGF-AB/BB. **C+D)** Protein expression levels of P21 and NF-κB in irradiated NP (**C)** and AF (**D)** cells treated with rhPDGF-AB/BB. n = 4 each group. One-way ANOVA with Dunnett post hoc testing was performed. The data is presented as mean with SD. *$p$< 0.05. **$p$< 0.01. ****$p$< 0.0001.

**Supplementary figure 1: Principle component analysis (PCA) of NP and AF samples treated with rhPDGF-AB and BB. A+B)** PCA plot of NP (**A**) cells and AF cell (**B**) showed the distinct cluster between untreated and treated samples. The clusters of PDGF-AB and BB samples were overlapping. NP: n = 5 each group. AF: n = 6 each group.

**Supplementary figure 2: Protein expression of PDGFRA was decreased in NP and AF samples treated with rhPDGF-AB and BB. A)** Representative images of western blot oof PDGFRA in NP (left) and AF (right) cells. **B)** Quantification of western blot results showing decreased PDGFRA expression in treated samples compared to the untreated group. NP: n=5; AF: n=6. One-way ANOVA with Dunnett post hoc testing was performed. The data is presented as mean with SD. *$p$< 0.05. **$p$< 0.01.

## Table captions

**Table 1:** Donor information.

Table 1. Donor information

| Grade | Age | Sex | Cell type |
|---|---|---|---|
| 4 | 67 | M | NP & AF |
| 5 | 61 | M | NP & AF |
| 5 | 61 | M | NP & AF |
| 4 or 5 | 65 | F | NP & AF |
| 4 or 5 | 81 | F | AF |
| 4 | 53 | F | AF |
| 4 | 64 | F | NP |
| 1 | 19 | M | NP & AF |
| 1 | 21 | M | NP & AF |
| 1 | 25 | F | NP & AF |
| 1 | 27 | F | NP & AF |

**Table 2:** Sequence of primers.

Table 2. Sequence of primers

| Gene | Primer sequence |
|---|---|
| *P21* | Forward: 5'-GAC ACCACT GGA GGG TGA CT-3'<br>Reverse: 5'-CAGGTC CAC ATG GTC TTC CT-3' |
| *P16* | Forward: 5'-CCAACGCACCGAATAGTTACG-3'<br>Reverse: 5'-GCGCTGCCCATCATCATG-3' |
| *IL6* | Forward: 5'-CCGGGAACGAAAGAGAAGCT-3'<br>Reverse: 5'-GCGCTTGTGGAGAAGGAGTT-3' |
| *CCNB1* | Forward: 5'-ACTGGGTCGGGAAGTCACTG-3'<br>Reverse: 5'-CATTCTTAGCCAGGTGCTGC-3' |
| *CCND1* | Forward: 5'-CTGTGCTGCGAAGTGGAAAC-3'<br>Reverse: 5'-TCTGTTTGTTCTCCTCCGCC-3' |
| *CASP3* | Forward: 5'-TGG TTC ATC CAG TCG CTT TG-3'<br>Reverse: 5'-ATT CTG TTG CCA CCT TTC G-3' |
| *MKI67* | Forward: 5'-ATTTGCTTCTGGCCTTCCCC-3'<br>Reverse: 5'-CCAAACAAGCAGGTGCTGAG-3' |
| *ACTB* | Forward: 5'-CTC TTC CAG CCT TCC TTC CT-3'<br>Reverse: 5'-AGC ACT GTG TTG GCG TAC AG-3' |
| *PDGFRA* | Forward: 5'-AGAAAACAACAGCGGCCTTT -3'<br>Reverse: 5'-CTACATCTGGGTCTGGCACA -3' |

## References


Chen J, Wei J-Q, Hong M-N, Zhang Z, Zhou H-D, Lu Y-Y, Zhang J, Guo Y-T, Chen X, Wang J-G, Gao P-J, Li X-D. 2023. Mitogen-Activated Protein Kinases Mediate Adventitial Fibroblast Activation and Neointima Formation via GATA4/Cyclin D1 Axis. *Cardiovasc Drugs Ther*. doi:10.1007/s10557-023-07428-1

Chen P-H, Chen X, He X. 2013. Platelet-derived growth factors and their receptors: structural and functional perspectives. *Biochim Biophys Acta* **1834**:2176–2186. doi:10.1016/j.bbapap.2012.10.015

Cherif H, Bisson DG, Mannarino M, Rabau O, Ouellet JA, Haglund L. 2020. Senotherapeutic drugs for human intervertebral disc degeneration and low back pain. *eLife* **9**. doi:10.7554/eLife.54693

Chin C-H, Chen S-H, Wu H-H, Ho C-W, Ko M-T, Lin C-Y. 2014. cytoHubba: identifying hub objects and sub-networks from complex interactome. *BMC Syst Biol* **8 Suppl 4**:S11. doi:10.1186/1752-0509-8-S4-S11

Chou M-Y, Li H-C. 2002. Genomic organization and characterization of the human type XXI collagen (COL21A1) gene. *Genomics* **79**:395–401. doi:10.1006/geno.2002.6712

Contreras O, Córdova-Casanova A, Brandan E. 2021. PDGF-PDGFR network differentially regulates the fate, migration, proliferation, and cell cycle progression of myogenic cells. *Cell Signal* **84**:110036. doi:10.1016/j.cellsig.2021.110036

Dittmar R, van Rijsbergen MM, Ito K. 2016. Moderately degenerated human intervertebral disks exhibit a less geometrically specific collagen fiber orientation distribution. *Global Spine J* **6**:439–446. doi:10.1055/s-0035-1564805

Feng C, Yang M, Lan M, Liu C, Zhang Y, Huang B, Liu H, Zhou Y. 2017. ROS: crucial intermediators in the pathogenesis of intervertebral disc degeneration. *Oxid Med Cell Longev* **2017**:5601593. doi:10.1155/2017/5601593

Feng Y, Egan B, Wang J. 2016. Genetic factors in intervertebral disc degeneration. *Genes Dis* **3**:178–185. doi:10.1016/j.gendis.2016.04.005

Freund A, Laberge R-M, Demaria M, Campisi J. 2012. Lamin B1 loss is a senescence-associated biomarker. *Mol Biol Cell* **23**:2066–2075. doi:10.1091/mbc.E11-10-0884

García-Olivas R, Vilaró S, Reina M, Castel S. 2007. PDGF-stimulated cell proliferation and migration of human arterial smooth muscle cells. Colocalization of PDGF isoforms with glycosaminoglycans. *Int J Biochem Cell Biol* **39**:1915–1929. doi:10.1016/j.biocel.2007.05.011

Gruber HE, Ingram JA, Davis DE, Hanley EN. 2009. Increased cell senescence is associated with decreased cell proliferation in vivo in the degenerating human annulus. *Spine J* **9**:210–215. doi:10.1016/j.spinee.2008.01.012

Gruber HE, Ingram JA, Norton HJ, Hanley EN. 2007. Senescence in cells of the aging and degenerating intervertebral disc: immunolocalization of senescence-associated beta-galactosidase in human and sand rat discs. *Spine* **32**:321–327. doi:10.1097/01.brs.0000253960.57051.de

Heldin C-H, Lennartsson J. 2013. Structural and functional properties of platelet-derived growth factor and stem cell factor receptors. *Cold Spring Harb Perspect Biol* **5**:a009100. doi:10.1101/cshperspect.a009100

Hida M, Fujita H, Ishikura K, Omori S, Hoshiya M, Awazu M. 2003. Eicosapentaenoic acid inhibits PDGF-induced mitogenesis and cyclin D1 expression via TGF-beta in mesangial cells. *J Cell Physiol* **196**:293–300. doi:10.1002/jcp.10298

Huang W, Hickson LJ, Eirin A, Kirkland JL, Lerman LO. 2022. Cellular senescence: the good, the bad and the unknown. *Nat Rev Nephrol* **18**:611–627. doi:10.1038/s41581-022-00601-z

Kudelko M, Chen P, Tam V, Zhang Y, Kong O-Y, Sharma R, Au TYK, To MK-T, Cheah KSE, Chan WCW, Chan D. 2021. PRIMUS: Comprehensive proteomics of mouse intervertebral discs that inform novel biology and relevance to human disease modelling. *Matrix Biology Plus* **12**:100082. doi:10.1016/j.mbplus.2021.100082

Lewis M. 2003. PRELP, collagen, and a theory of Hutchinson-Gilford progeria. *Ageing Res Rev* **2**:95–105. doi:10.1016/S1568-1637(02)00044-2

Lim S, An SB, Jung M, Joshi HP, Kumar H, Kim C, Song SY, Lee J-R, Kang M, Han I, Kim B-S. 2022. Local delivery of senolytic drug inhibits intervertebral disc degeneration and restores intervertebral disc structure. *Adv Healthc Mater* **11**:e2101483. doi:10.1002/adhm.202101483

Liu-Chittenden Y, Jain M, Gaskins K, Wang S, Merino MJ, Kotian S, Kumar Gara S, Davis S, Zhang L, Kebebew E. 2017. RARRES2 functions as a tumor suppressor by promoting β-catenin phosphorylation/degradation and inhibiting p38 phosphorylation in adrenocortical carcinoma. *Oncogene* **36**:3541–3552. doi:10.1038/onc.2016.497

Li H, Yan R, Chen W, Ding X, Liu J, Chen G, Zhao Q, Tang Y, Lv S, Liu S, Yu Y. 2021. Long non coding RNA SLC26A4-AS1 exerts antiangiogenic effects in human glioma by upregulating NPTX1 via NFKB1 transcriptional factor. *FEBS J* **288**:212–228. doi:10.1111/febs.15325

Mannarino M, Cherif H, Li L, Sheng K, Rabau O, Jarzem P, Weber MH, Ouellet JA, Haglund L. 2021. Toll-like receptor 2 induced senescence in intervertebral disc cells of patients with back pain can be attenuated by o-vanillin. *Arthritis Res Ther* **23**:117. doi:10.1186/s13075-021-02504-z

Mannarino M, Wu-Martinez O, Sheng K, Li L, Navarro-Ramirez R, Jarzem P, Ouellet JA, Cherif H, Haglund L. 2023. Senolytic Combination Treatment Is More Potent Than Single Drugs in Reducing Inflammatory and Senescence Burden in Cells from Painful Degenerating IVDs. *Biomolecules* **13**. doi:10.3390/biom13081257

Martin-Garrido A, Williams HC, Lee M, Seidel-Rogol B, Ci X, Dong J-T, Lassègue B, Martín AS, Griendling KK. 2013. Transforming growth factor β inhibits platelet derived growth factor-induced vascular smooth muscle cell proliferation via Akt-independent, Smad-mediated cyclin D1 downregulation. *PLoS ONE* **8**:e79657. doi:10.1371/journal.pone.0079657

Mavillard F, Servian-Morilla E, Dofash L, Rojas-Marcos I, Folland C, Monahan G, Gutierrez-Gutierrez G, Rivas E, Hernández-Lain A, Valladares A, Cantero G, Morales JM, Laing NG, Paradas C, Ravenscroft G, Cabrera-Serrano M. 2023. Ablation of the carboxy-terminal end of MAMDC2 causes a distinct muscular dystrophy. *Brain* **146**:5235–5248. doi:10.1093/brain/awad256

Novais EJ, Tran VA, Johnston SN, Darris KR, Roupas AJ, Sessions GA, Shapiro IM, Diekman BO, Risbud MV. 2021. Long-term treatment with senolytic drugs Dasatinib and Quercetin ameliorates age-dependent intervertebral disc degeneration in mice. *Nat Commun* **12**:5213. doi:10.1038/s41467-021-25453-2

Paglia DN, Singh H, Karukonda T, Drissi H, Moss IL. 2016. PDGF-BB Delays Degeneration of the Intervertebral Discs in a Rabbit Preclinical Model. *Spine* **41**:E449-58. doi:10.1097/BRS.0000000000001336

Presciutti SM, Paglia DN, Karukonda T, Soung DY, Guzzo R, Drissi H, Moss IL. 2014. PDGF-BB inhibits intervertebral disc cell apoptosis in vitro. *J Orthop Res* **32**:1181–1188. doi:10.1002/jor.22638

Rashid MM, Runci A, Russo MA, Tafani M. 2015. Muscle Lim Protein (MLP)/CSRP3 at the crossroad between mechanotransduction and autophagy. *Cell Death Dis* **6**:e1940. doi:10.1038/cddis.2015.308

Ruiz-Fernández C, González-Rodríguez M, Abella V, Francisco V, Cordero-Barreal A, Ait Eldjoudi D, Farrag Y, Pino J, Conde-Aranda J, González-Gay MÁ, Mera A, Mobasheri A, García-Caballero L, Gándara-Cortés M, Lago F, Scotece M, Gualillo O. 2022. WISP-2 modulates the induction of inflammatory mediators and cartilage catabolism in chondrocytes. *Lab Invest* **102**:989–999. doi:10.1038/s41374-022-00793-9

Silagi ES, Schipani E, Shapiro IM, Risbud MV. 2021. The role of HIF proteins in maintaining the metabolic health of the intervertebral disc. *Nat Rev Rheumatol* **17**:426–439. doi:10.1038/s41584-021-00621-2

Silagi ES, Schoepflin ZR, Seifert EL, Merceron C, Schipani E, Shapiro IM, Risbud MV. 2018. Bicarbonate Recycling by HIF-1-Dependent Carbonic Anhydrase Isoforms 9 and 12 Is Critical in Maintaining Intracellular pH and Viability of Nucleus Pulposus Cells. *J Bone Miner Res* **33**:338–355. doi:10.1002/jbmr.3293

Silwal P, Nguyen-Thai AM, Mohammad HA, Wang Y, Robbins PD, Lee JY, Vo NV. 2023. Cellular senescence in intervertebral disc aging and degeneration: molecular mechanisms and potential therapeutic opportunities. *Biomolecules* **13**. doi:10.3390/biom13040686

Singhmar P, Trinh RTP, Ma J, Huo X, Peng B, Heijnen CJ, Kavelaars A. 2020. The fibroblast-derived protein PI16 controls neuropathic pain. *Proc Natl Acad Sci USA* **117**:5463–5471. doi:10.1073/pnas.1913444117

Song C, Hu P, Peng R, Li F, Fang Z, Xu Y. 2024. Bioenergetic dysfunction in the pathogenesis of intervertebral disc degeneration. *Pharmacol Res* **202**:107119. doi:10.1016/j.phrs.2024.107119

Song E-L, Hou Y-P, Yu S-P, Chen S-G, Huang J-T, Luo T, Kong L-P, Xu J, Wang H-Q. 2011. EFEMP1 expression promotes angiogenesis and accelerates the growth of cervical cancer in vivo. *Gynecol Oncol* **121**:174–180. doi:10.1016/j.ygyno.2010.11.004

Tang Y, Li M, Wang J, Pan Y, Wu F-X. 2015. CytoNCA: a cytoscape plugin for centrality analysis and evaluation of protein interaction networks. *BioSystems* **127**:67–72. doi:10.1016/j.biosystems.2014.11.005

Veroutis D, Kouroumalis A, Lagopati N, Polyzou A, Chamilos C, Papadodima S, Evangelou K, Gorgoulis VG, Kletsas D. 2021. Evaluation of senescent cells in intervertebral discs by lipofuscin staining. *Mech Ageing Dev* **199**:111564. doi:10.1016/j.mad.2021.111564

Vince JW, Reithmeier RA. 1998. Carbonic anhydrase II binds to the carboxyl terminus of human band 3, the erythrocyte C1-/HCO3- exchanger. *J Biol Chem* **273**:28430–28437. doi:10.1074/jbc.273.43.28430

Wang D-K, Zheng H-L, Zhou W-S, Duan Z-W, Jiang S-D, Li B, Zheng X-F, Jiang L-S. 2022. Mitochondrial Dysfunction in Oxidative Stress-Mediated Intervertebral Disc Degeneration. *Orthop Surg* **14**:1569–1582. doi:10.1111/os.13302

Wang F, Cai F, Shi R, Wang XH, Wu XT. 2016. Aging and age related stresses: a senescence mechanism of intervertebral disc degeneration. *Osteoarthr Cartil* **24**:398–408. doi:10.1016/j.joca.2015.09.019

Weibrich G, Kleis WKG, Hafner G, Hitzler WE. 2002. Growth factor levels in platelet-rich plasma and correlations with donor age, sex, and platelet count. *J Craniomaxillofac Surg* **30**:97–102. doi:10.1054/jcms.2002.0285

Wu T, Hu E, Xu S, Chen M, Guo P, Dai Z, Feng T, Zhou L, Tang W, Zhan L, Fu X, Liu S, Bo X, Yu G. 2021. clusterProfiler 4.0: A universal enrichment tool for interpreting omics data. *Innovation (Camb)* **2**:100141. doi:10.1016/j.xinn.2021.100141

Zhang C, Gordon MD, Joseph KM, Diaz-Hernandez ME, Drissi H, Illien-Jünger S. 2024. Differential efficacy of two small molecule PHLPP inhibitors to promote nucleus Pulposus cell health. *JOR Spine* **7**:e1306. doi:10.1002/jsp2.1306

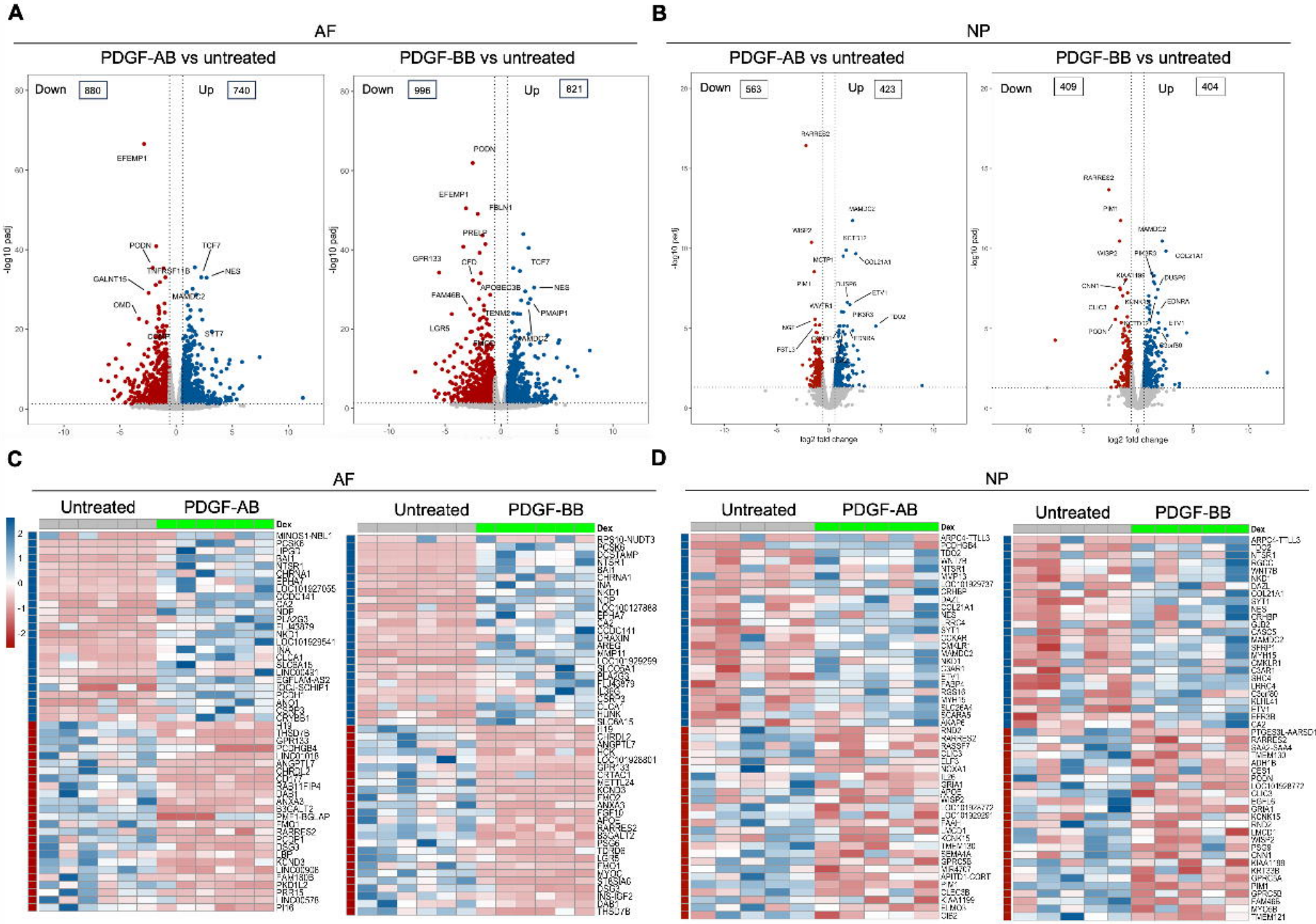
A
AF
PDGF-AB vs untreated
Down 880
Up 740
PDGF-BB vs untreated
Down 996
Up 821
-log10 padj
B
NP
PDGF-AB vs untreated
Down 563
Up 423
PDGF-BB vs untreated
Down 409
Up 404
log2 fold change
C
AF
Untreated
PDGF-AB
PDGF-BB
Dex
D
NP
Untreated
PDGF-AB
PDGF-BB
Dex

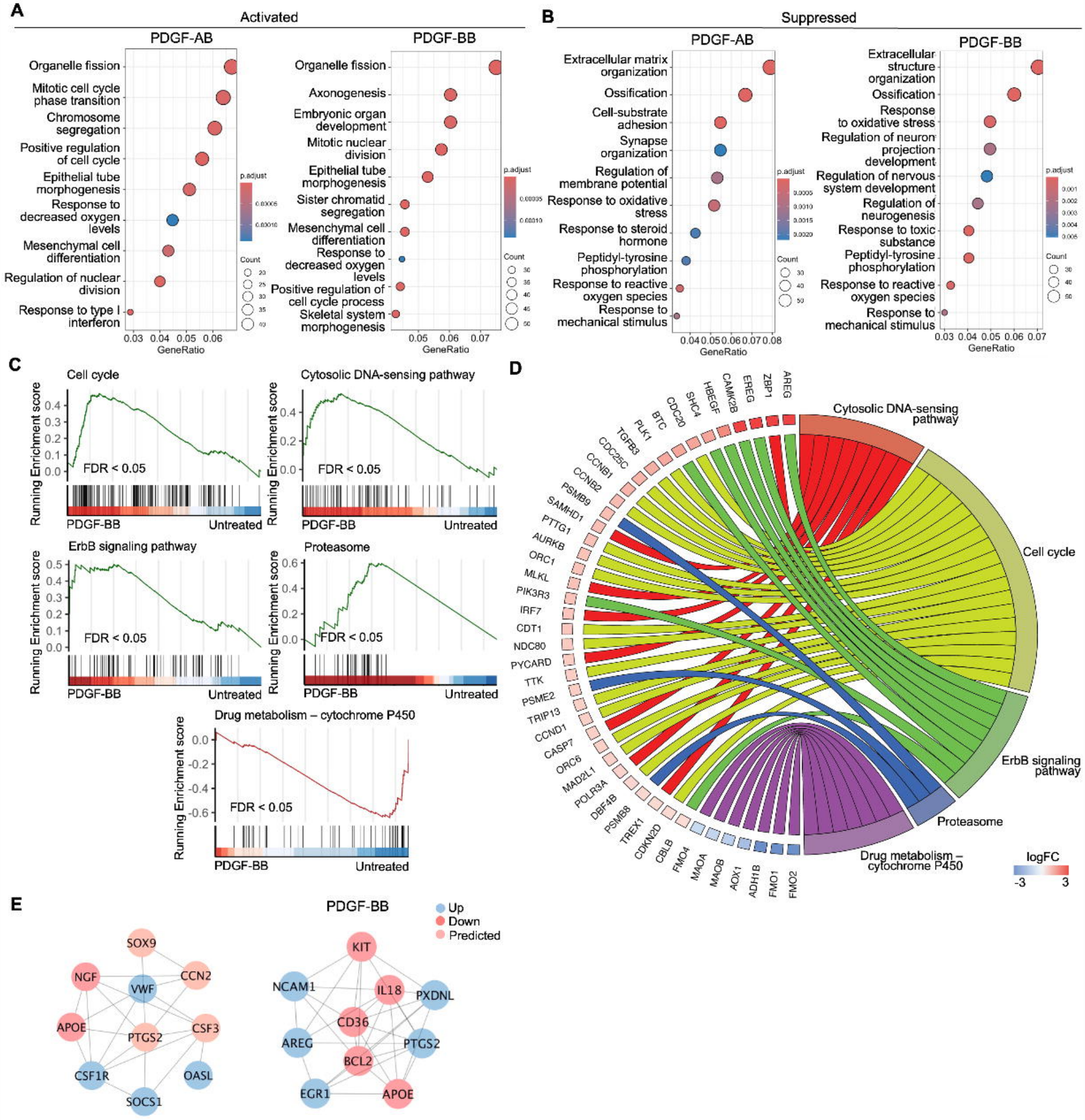
A
Activated
PDGF-AB
Organelle fission
Mitotic cell cycle phase transition
Chromosome segregation
Positive regulation of cell cycle
Epithelial tube morphogenesis
Response to decreased oxygen levels
Mesenchymal cell differentiation
Regulation of nuclear division
Response to type I interferon
GeneRatio
PDGF-BB
Organelle fission
Axonogenesis
Embryonic organ development
Mitotic nuclear division
Epithelial tube morphogenesis
Sister chromatid segregation
Mesenchymal cell differentiation
Response to decreased oxygen levels
Positive regulation of cell cycle process
Skeletal system morphogenesis
GeneRatio
p.adjust
Count
B
Suppressed
PDGF-AB
Extracellular matrix organization
Ossification
Cell-substrate adhesion
Synapse organization
Regulation of membrane potential
Response to oxidative stress
Response to steroid hormone
Peptidyl-tyrosine phosphorylation
Response to reactive oxygen species
Response to mechanical stimulus
GeneRatio
PDGF-BB
Extracellular structure organization
Ossification
Response to oxidative stress
Regulation of neuron projection development
Regulation of nervous system development
Regulation of neurogenesis
Response to toxic substance
Peptidyl-tyrosine phosphorylation
Response to reactive oxygen species
Response to mechanical stimulus
GeneRatio
C
Cell cycle
Cytosolic DNA-sensing pathway
ErbB signaling pathway
Proteasome
Drug metabolism – cytochrome P450
Running Enrichment score
FDR < 0.05
PDGF-BB
Untreated
D
Cytosolic DNA-sensing pathway
Cell cycle
ErbB signaling pathway
Proteasome
Drug metabolism – cytochrome P450
AREG
ZBP1
EREG
CAMK2B
HBEGF
SHC4
CDC20
BTC
PLK1
TGFB3
CDC25C
CCNB1
CCNB2
PSMB9
SAMHD1
PTTG1
AURKB
ORC1
MLKL
PIK3R3
IRF7
CDT1
NDC80
PYCARD
TTK
PSME2
TRIP13
CCND1
CASP7
ORC6
MAD2L1
POLR3A
DBF4B
PSMB8
TREX1
CDKN2D
CBLB
FMO4
MAOA
MAOB
AOX1
ADH1B
FMO1
FMO2
logFC
-3
3
E
PDGF-BB
Up
Down
Predicted
SOX9
NGF
CCN2
VWF
APOE
PTGS2
CSF3
CSF1R
OASL
SOCS1
KIT
NCAM1
IL18
PXDNL
CD36
AREG
PTGS2
BCL2
EGR1
APOE

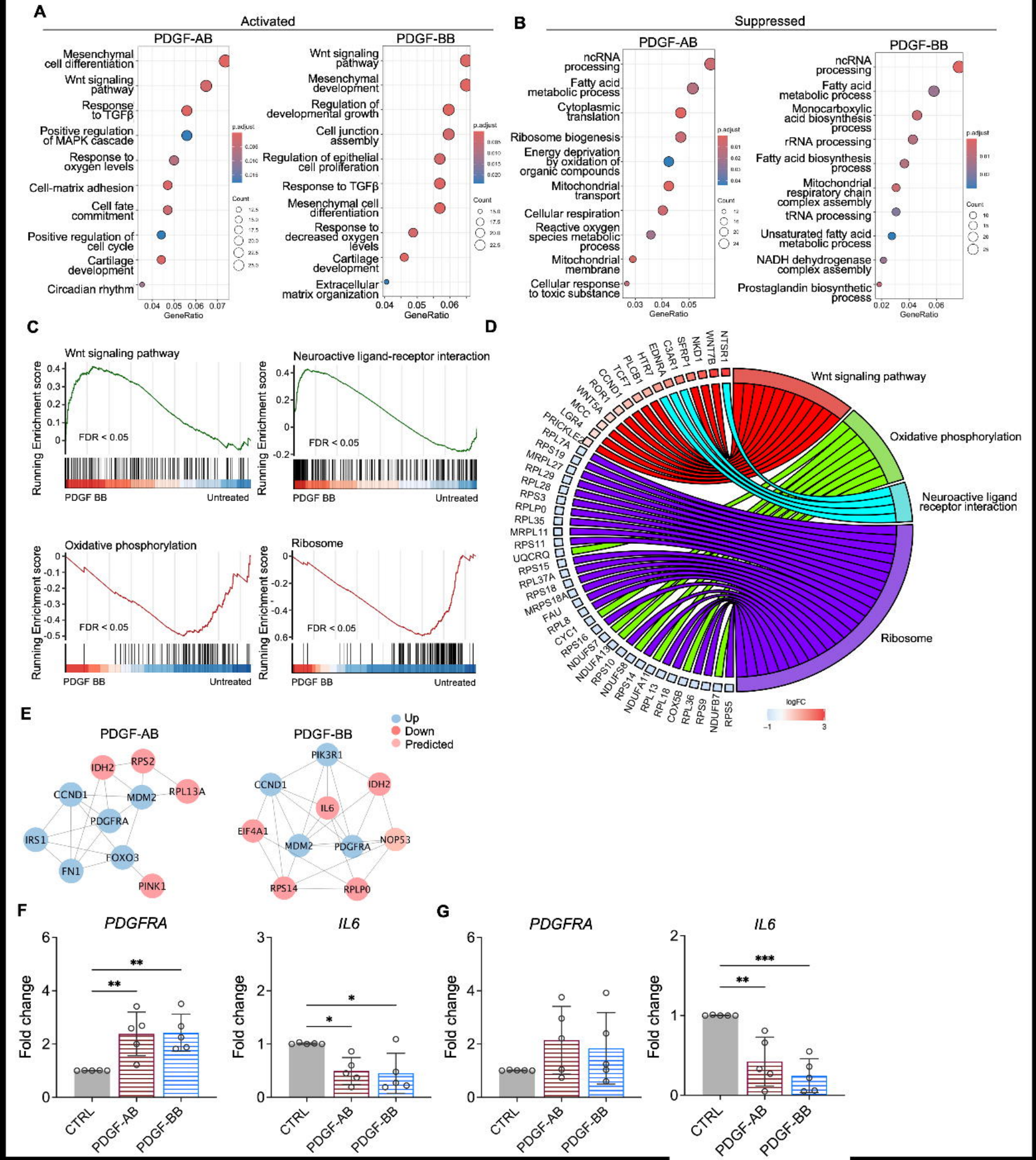
A
Activated
PDGF-AB
Mesenchymal cell differentiation
Wnt signaling pathway
Response to TGFβ
Positive regulation of MAPK cascade
Response to oxygen levels
Cell-matrix adhesion
Cell fate commitment
Positive regulation of cell cycle
Cartilage development
Circadian rhythm
GeneRatio
PDGF-BB
Wnt signaling pathway
Mesenchymal development
Regulation of developmental growth
Cell junction assembly
Regulation of epithelial cell proliferation
Response to TGFβ
Mesenchymal cell differentiation
Response to decreased oxygen levels
Cartilage development
Extracellular matrix organization
GeneRatio
B
Suppressed
PDGF-AB
ncRNA processing
Fatty acid metabolic process
Cytoplasmic translation
Ribosome biogenesis
Energy deprivation by oxidation of organic compounds
Mitochondrial transport
Cellular respiration
Reactive oxygen species metabolic process
Mitochondrial membrane
Cellular response to toxic substance
GeneRatio
PDGF-BB
ncRNA processing
Fatty acid metabolic process
Monocarboxylic acid biosynthesis process
rRNA processing
Fatty acid biosynthesis process
Mitochondrial respiratory chain complex assembly
tRNA processing
Unsaturated fatty acid metabolic process
NADH dehydrogenase complex assembly
Prostaglandin biosynthetic process
GeneRatio
C
Wnt signaling pathway
Neuroactive ligand-receptor interaction
Oxidative phosphorylation
Ribosome
Running Enrichment score
FDR < 0.05
PDGF BB
Untreated
D
Wnt signaling pathway
Oxidative phosphorylation
Neuroactive ligand receptor interaction
Ribosome
NTSR1
WNT7B
NKD1
SFRP1
C3AR1
EDNRA
HTR7
PLCB1
TCF7
CCND1
ROR1
WNT5A
MCC
LGR4
PRICKLE2
RPL7A
RPS19
MRPL27
RPL29
RPL28
RPS3
RPLP0
RPL35
MRPL11
RPS11
UQCRQ
RPS15
RPL37A
RPS18
MRPS18A
FAU
RPL8
CYC1
RPS16
NDUFS7
NDUFA13
RPS10
NDUFS8
RPS14
NDUFA11
RPL13
RPL18
COX5B
RPL36
RPS9
NDUFB7
RPS5
logFC
-1
3
E
Up
Down
Predicted
PDGF-AB
IDH2
RPS2
CCND1
MDM2
RPL13A
PDGFRA
IRS1
FOXO3
FN1
PINK1
PDGF-BB
PIK3R1
CCND1
IDH2
IL6
EIF4A1
MDM2
PDGFRA
NOP53
RPS14
RPLP0
F
PDGFRA
IL6
Fold change
CTRL
PDGF-AB
PDGF-BB
G
PDGFRA
IL6
Fold change
CTRL
PDGF-AB
PDGF-BB

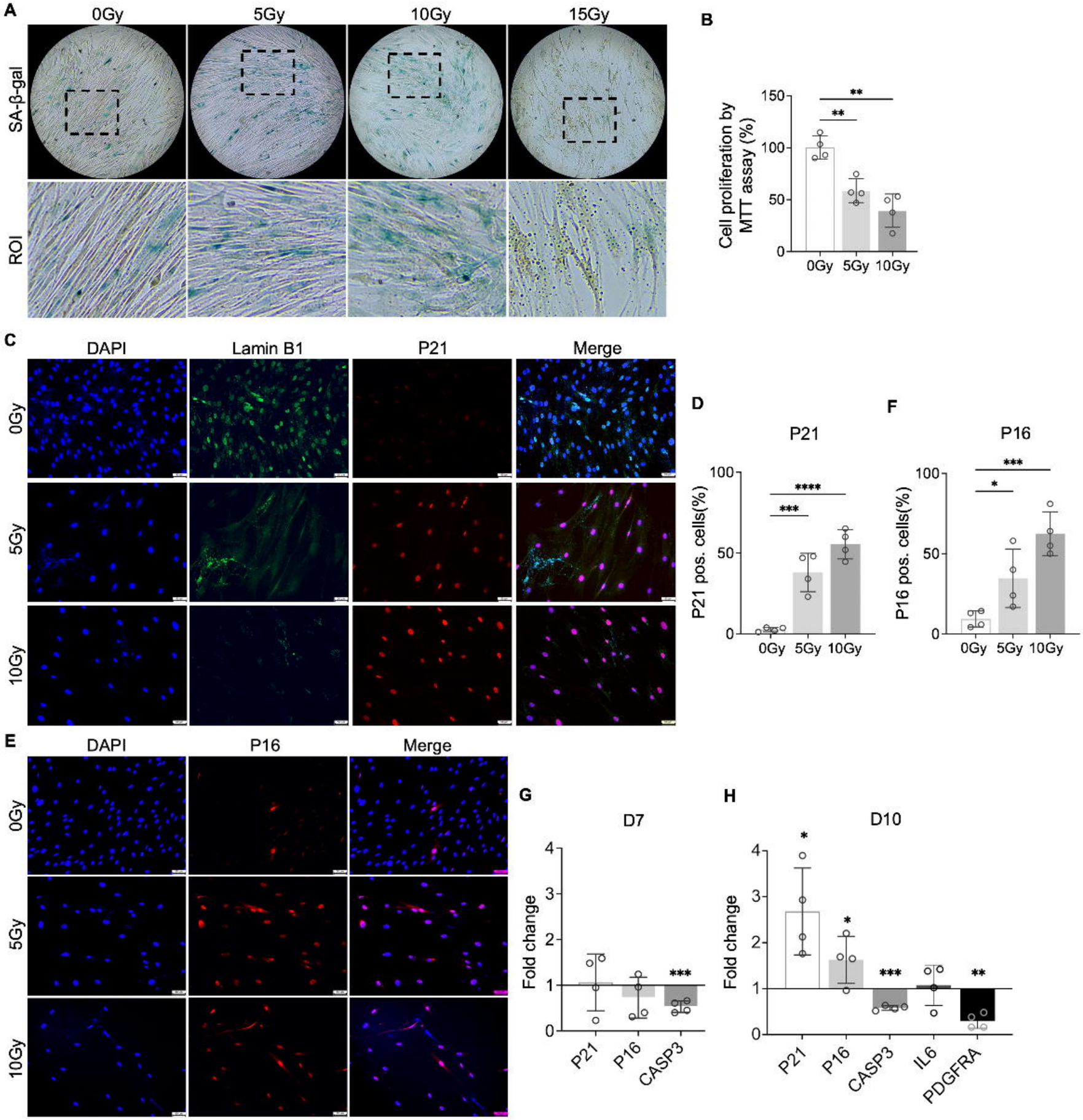
A
0Gy
5Gy
10Gy
15Gy
SA-β-gal
ROI
B
Cell proliferation by MTT assay (%)
150
100
50
0
**
**
0Gy
5Gy
10Gy
C
DAPI
Lamin B1
P21
Merge
0Gy
5Gy
10Gy
D
P21
P21 pos. cells(%)
100
50
0
****
***
0Gy
5Gy
10Gy
F
P16
P16 pos. cells(%)
100
50
0
***
*
0Gy
5Gy
10Gy
E
DAPI
P16
Merge
0Gy
5Gy
10Gy
G
D7
Fold change
4
3
2
1
0
***
P21
P16
CASP3
H
D10
Fold change
4
3
2
1
0
*
*
***
**
P21
P16
CASP3
IL6
PDGFRA

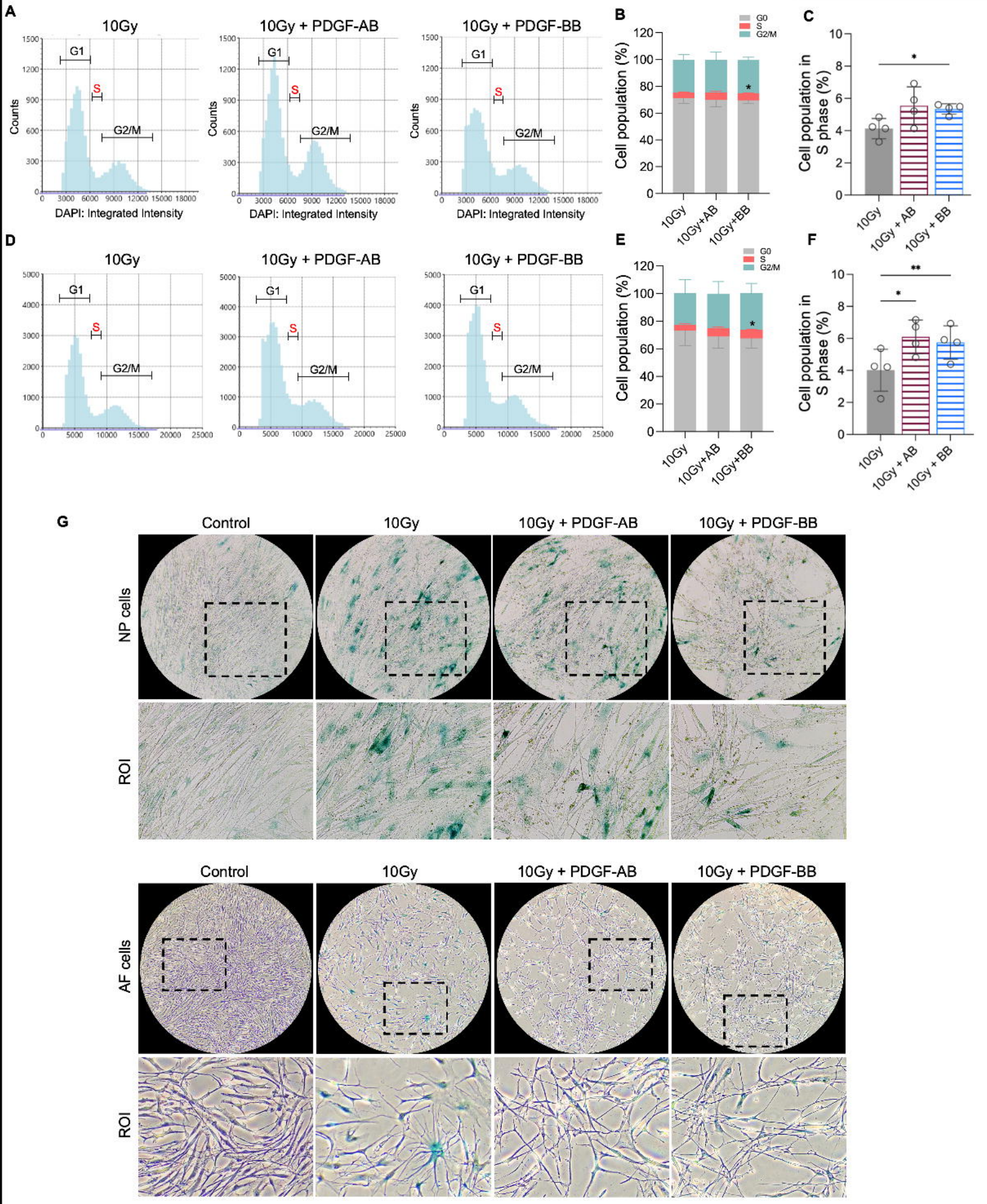
A
10Gy
10Gy + PDGF-AB
10Gy + PDGF-BB
G1
S
G2/M
Counts
DAPI: Integrated Intensity
B
G0
S
G2/M
Cell population (%)
10Gy
10Gy+AB
10Gy+BB
C
Cell population in S phase (%)
10Gy + AB
10Gy + BB
D
E
F
G
Control
NP cells
ROI
AF cells

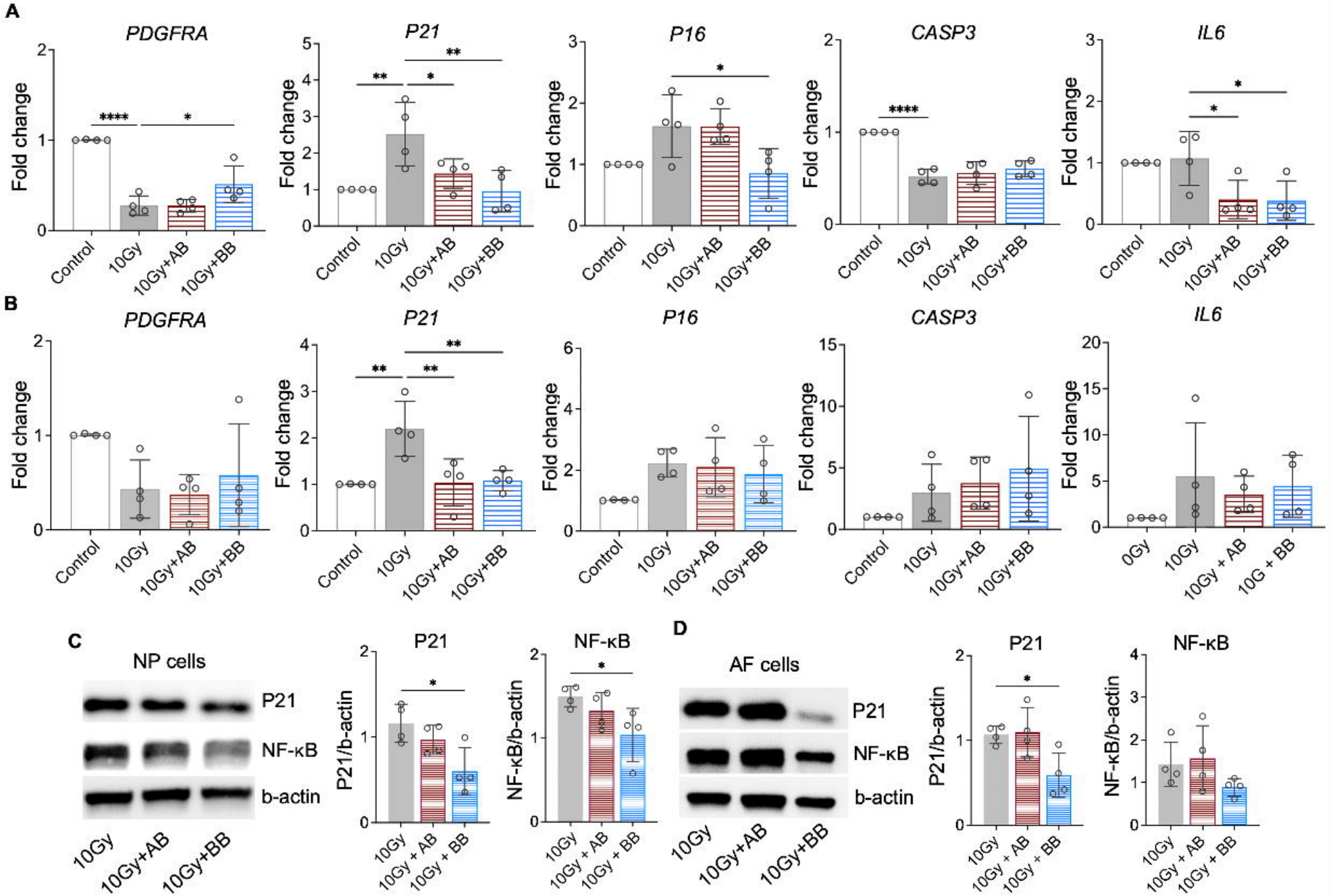
A
PDGFRA
P21
P16
CASP3
IL6
Fold change
Control
10Gy
10Gy+AB
10Gy+BB
B
0Gy
10Gy + AB
10G + BB
C
NP cells
P21
NF-κB
b-actin
P21/b-actin
NF-κB/b-actin
10Gy + AB
10Gy + BB
D
AF cells